Pushing the boundaries of chemistry?
It takes #HumanChemistry

Make your curiosity and talent as a chemist matter to the world with a specialty chemicals leader. Together, we combine cutting-edge science with engineering expertise to create solutions that answer real-world problems. Find out how our approach to technology creates more opportunities for growth, and see what chemistry can do for you at:

evonik.com/career

EVONIK
Leading Beyond Chemistry

Perovskite Origami for Programmable Microtube Lasing

Haiyun Dong, Christian Niclaas Saggau, Minshen Zhu, Jie Liang, Shengkai Duan, Xiaoyu Wang, Hongmei Tang, Yin Yin, Xiaoxia Wang, Jiawei Wang, Chunhuan Zhang, Yong Sheng Zhao,* Libo Ma,* and Oliver G. Schmidt*

Metal halide perovskites are promising materials for optoelectronic and photonic applications ranging from photovoltaics to laser devices. However, current perovskite devices are constrained to simple low-dimensional structures suffering from limited design freedom and holding up performance improvement and functionality upgrades. Here, a micro-origami technique is developed to program 3D perovskite microarchitectures toward a new type of microcavity laser. The design flexibility in 3D supports not only outstanding laser performance such as low threshold, tunable output, and high stability but also yields new functionalities like 3D confined mode lasing and directional emission in, for example, laser "array-in-array" systems. The results represent a significant step forward toward programmable microarchitectures that take perovskite optoelectronics and photonics into the 3D era.

1. Introduction

Metal halide perovskites are an emerging class of semiconductors for optoelectronics and photonics, finding advanced applications in solar cells, photodetectors, light-emitting diodes, and lasers.[1] Through rational engineering of composition and structure, great progress has been made in improving the performance and expanding the functionalities of perovskite devices.[2] Mesoscopic perovskite structures are particularly appealing for photonic applications as they accommodate intriguing photonic phenomena, such as optical resonance, nonlinearity, and quantum effects.[3] Typical mesoscopic perovskite structures include directly synthesized or lithographically patterned 0D nanocrystals, 1D nanowires, and 2D microplates with efficient luminescence and lasing originating from strong excitonic and photonic confinement.[4] However, current perovskite mesostructures are restricted to in-plane configurations with only little on-chip design freedom. Hence, the development of 3D perovskite microarchitectures with programmable geometries and new emission properties would open up new perspectives for perovskite optoelectronic integration and photonic applications.

Microscale origami (micro-origami) is an art of folding 2D nanomembranes into 3D microarchitectures,[5] offering a versatile route to 3D microdevices with new characteristics and functionalities. Among various 3D microarchitectures, self-assembled Swiss-roll microtubes are particularly attractive as they show broad application potential in optoelectronics, photonics, magnetics, microrobotics, and more.[6] However, it remains a great challenge to incorporate various active optoelectronic and photonic materials into the microtube structures in a controllable fashion so far. In this work, we design a versatile micro-origami approach to programmatically assemble perovskite thin films into customized microtubes for

H. Dong, C. N. Saggau, M. Zhu, S. Duan, X. Wang, H. Tang,
Y. Yin, X. Wang, J. Wang, L. Ma, O. G. Schmidt
Institute for Integrative Nanosciences
Leibniz IFW Dresden
01069 Dresden, Germany
E-mail: l.ma@ifw-dresden.de; o.schmidt@ifw-dresden.de
J. Liang, C. Zhang, Y. S. Zhao
Key Laboratory of Photochemistry
Institute of Chemistry
Chinese Academy of Sciences
Beijing 100190, China
E-mail: yszhao@iccas.ac.cn

The ORCID identification number(s) for the author(s) of this article can be found under https://doi.org/10.1002/adfm.202109080.

S. Duan, H. Tang, O. G. Schmidt
Material Systems for Nanoelectronics
TU Chemnitz
09107 Chemnitz, Germany
S. Duan, H. Tang, O. G. Schmidt
Research Center for Materials, Architectures and Integration of Nanomembranes
TU Chemnitz
09126 Chemnitz, Germany
X. Wang, O. G. Schmidt
Nanophysics, Faculty of Physics
TU Dresden
01062 Dresden, Germany
Y. Yin
School of Materials Science and Engineering
Jiangsu University
Zhenjiang 212013, China
J. Wang
School of Electronic and Information Engineering
Harbin Institute of Technology, Shenzhen
Shenzhen 518055, China

the construction of a new generation of 3D microcavity lasers. The 3D perovskite microtube cavities not only show superior laser performance, such as low threshold, directional emission, tunable output, and high stability, but also produce novel laser features, such as laser array-in-array emission and 3D mode lasing. The 3D microcavity laser design promises intriguing application potential for 3D coherent light delivery, enhanced optical sensing, and 3D photonic integration. Our investigation establishes a platform for extending the functionality and application of metal halide perovskites into the third dimension, and by demonstrating efficient lasing, we leverage perovskite optoelectronics and photonics into a new era.

2. Results and Discussion

The key to micro-origami design lies in the clever construction of differentially strained bilayers that provide the driving force for the self-assembly of thin solid films into 3D microarchitectures.[5] Here, smooth films of diverse perovskites are obtained by anti-solvent assisted spin-coating (Figure S1, Supporting Information).[7] As the perovskite film usually contains tensile strain,[8] we introduce a compressively strained film below to construct the functional bilayer where the differential strain drives the top and bottom layers to contract and expand, respectively, causing the whole film to roll up into a Swiss-roll tubular microstructure (**Figure 1**a).[9] Perovskites are excellent optical gain media with large optical gain coefficients and chemically tailorable bandgaps.[4b,c] The microtube architectures with circular cross-sections form 3D microcavities supporting whispering-gallery-mode (WGM) optical resonances (Figure S2, Supporting Information).[10] Therefore, the perovskite microtubes can function as WGM lasers by simultaneously providing high optical gain and effective optical feedback.

Figure 1b schematically shows our designed micro-origami approach for the fabrication of the perovskite microtube lasers. The fabrication starts with successive depositions of amorphous silicon (Si), aluminum oxide (Al_2O_3), silicon nitride (Si_3N_4), cesium lead halide ($CsPbX_3$), and aluminum oxide onto a silicon dioxide (SiO_2) substrate (Figure 1b-I; Figure S3a, Supporting Information; also see Experimental Section for further details). The compressively strained silicon nitride together with the tensile strained perovskite constitutes the differentially strained bilayer. The silicon film serves as a sacrificial layer that can be rapidly removed by xenon difluoride. Two layers of aluminum oxide protect the strained bilayer from corrosion by the solvents and etchants during the film patterning and film release. The strained bilayer and sacrificial layer are successively patterned through standard photolithography (Figure 1bII; Figure S3b,c, Supporting Information). The sacrificial layer pattern is a little wider than the strained bilayer to define where to start etching the sacrificial layer for releasing the strained bilayer. The patterned films are then passivated by coating an aluminum oxide thin film (Figure 1b-III) to anchor the strained bilayer to the substrate. After that, the extra strip of the sacrificial layer is exposed by removing the passivation layer via photolithography (Figure 1b-IV; Figure S3d, Supporting Information). This strip window defines the starting edge to directionally roll up the strained bilayer. To do so, the silicon sacrificial layer is selectively

removed by xenon difluoride etching from the starting edge. Driven by strain relaxation, the patterned film self-assembles into a compact 3D Swiss roll microtube with well-controlled rolling direction and length (Figure 1b-V).

Figure 1c shows the origami process of a patterned Al_2O_3/ Si_3N_4/$CsPbBr_3$/Al_2O_3 film at different stages. With the gradual removal of the silicon sacrificial layer, the strained film spontaneously curls up and rolls into a microtube. The roll-up from a U-shaped pattern produces a free-standing optical microtube cavity with strong light confinement as its middle segment is suspended above the substrate by ≈1 µm effectively suppressing optical leakage into the substrate.

All fabrication processes involved in the origami approach are silicon-compatible and enable wafer-scale fabrication of microtube lasers. **Figure 2**a shows a 2-inch silicon wafer containing ≈2 × 10⁴ $CsPbBr_3$ perovskite microtubes with a yield over 99%. All perovskite microtubes on the wafer exhibit almost the same morphology with lengths of 240 µm and diameters of 20 µm (Figure 2a, inset; Figure S4, Supporting Information). Moreover, the structures of the perovskite microtubes can be well-controlled by changing the origami parameters. For example, the length and diameter of the perovskite microtubes can be precisely controlled by designing the strained bilayer pattern and thickness, respectively (Figures S5 and S6, Supporting Information). The structure control of the microtube cavity can be utilized for programming the laser characteristics.[11] Scanning electron microscopy (SEM) image in lateral view demonstrates the hollow structure of the origami perovskite microtube (Figure S7, Supporting Information). In addition, the perovskite microtube has a smooth surface and suspended middle segment (Figure 2b; Figure S8, Supporting Information), which suppresses both optical scattering losses and optical leakage into the substrate, respectively, and therefore facilitates the occurrence of low-threshold lasing.

Energy-dispersive X-ray spectroscopy (EDS) images verify the components of the microtubes, that is, the Al_2O_3 protection layer, Si_3N_4 strained layer, and $CsPbBr_3$ active layer (Figure 2c). The molar ratio of Cs, Pb, and Br in the perovskite film incorporated in the microtube is 1:1:3.2 conforming to the $CsPbBr_3$ stoichiometry. The X-ray diffraction (XRD) pattern shows that the $CsPbBr_3$ perovskite film in the microtube is indexed to the orthorhombic phase (Figure 2d), which is the same as that of the perovskite film before origami (Figure S1, Supporting Information). The successful roll-up and excellent protection of the perovskite film indicate that our origami approach can be applied to a wide range of materials, opening up an avenue toward 3D optoelectronics and photonics.

As shown in **Figure 3**a, the $CsPbBr_3$ perovskite microtube cavities exhibit strong photoluminescence (PL) with great potential for low-threshold lasing. Optically pumped emission spectra were measured by a far-field micro-PL system (Figures S9 and S10, Supporting Information). A beam-expanded pulsed laser (400 nm, 100 fs, 1 kHz) was used as a nearly uniform pump source to excite an individual perovskite microtube. At low pump fluence ($P < 1.86$ µJ cm⁻²), the perovskite microtube shows broad spontaneous emission (Figure 3b). With increasing pump fluence ($P \geq 1.86$ µJ cm⁻²), the emission develops into a set of sharp laser peaks. The nonlinear response of the emission intensity to the pump fluence marks the onset of
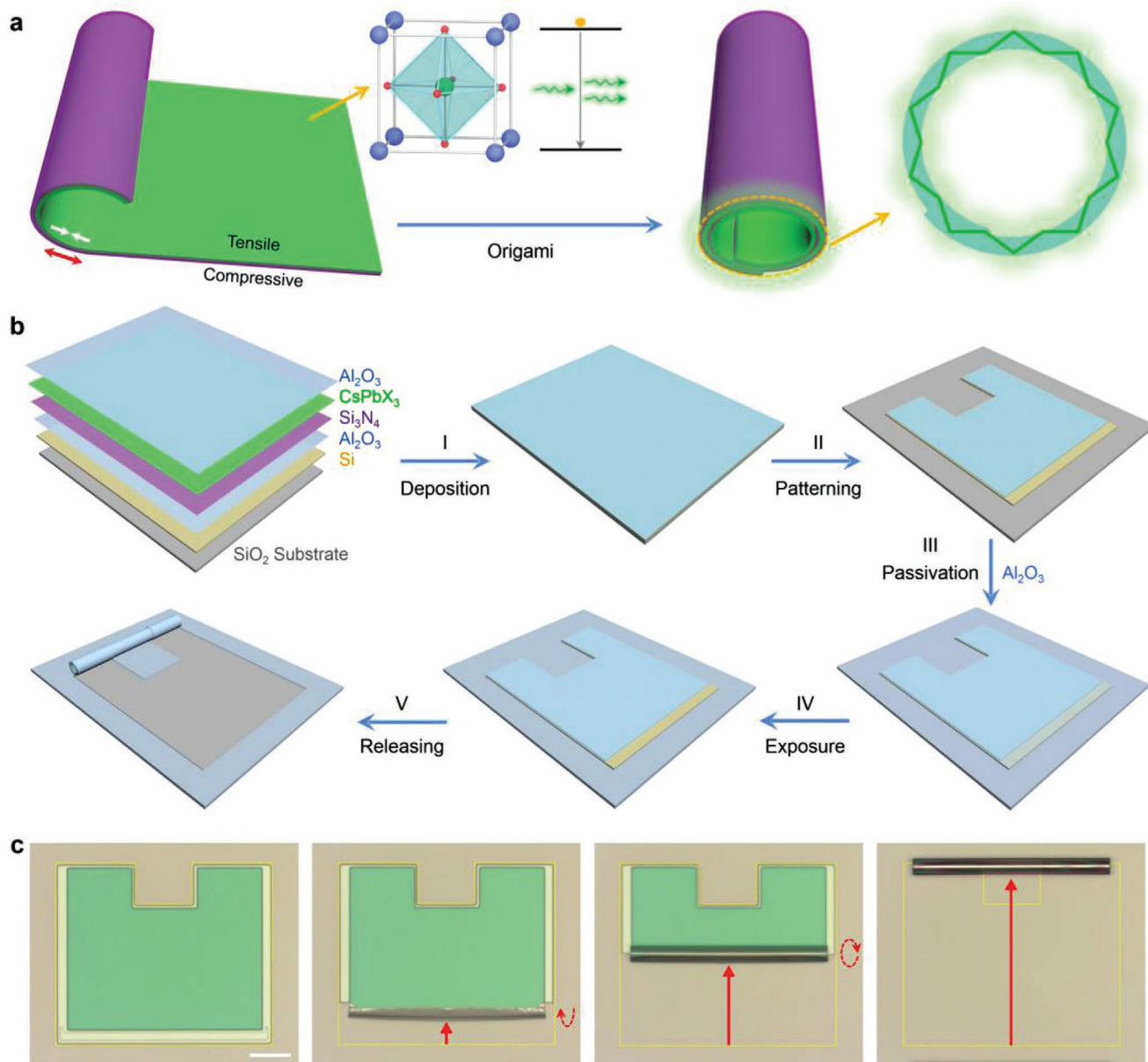
Figure 1. Metal halide perovskite micro-origami. a) Design of perovskite origami toward 3D microtube lasers. Left inset: schematic diagram of the perovskite unit cell and the stimulated emission transition. Right inset: schematic WGM resonance confined to the microtube cross-section. b) Schematic diagram showing the fabrication flow of the perovskite microtube laser. The fabrication flow includes the deposition, patterning, and passivation of the functional multilayers, opening of the etching window, and selective removal of the sacrificial layer. c) Bright-field microscopy images of a patterned film (5 nm Al_2O_3/45 nm Si_3N_4/45 nm $CsPbBr_3$/5 nm Al_2O_3) at different origami stages. Scale bar is 50 µm. With the gradual removal of the silicon sacrificial layer, the strained bilayer spontaneously rolls up into a microtube.

lasing,[12] with a lasing threshold of ≈1.86 µJ cm^{-2} (Figure 3c). This lasing threshold is among the lowest values for inorganic perovskite lasers.[13] We attribute this accomplishment to the smooth and free-standing microtube structure with minimized scattering loss and suppressed optical leakage into the substrate. The excited-state dynamics of the perovskite microtube laser was investigated by time-resolved photoluminescence (Figure S11, Supporting Information). At low pump fluence ($P = 0.60\ P_{th}$), the spontaneous emission follows an exponential decay with a lifetime (τ) of 660 ps. When

the pump fluence exceeds the lasing threshold ($P = 1.55\ P_{th}$), an ultrafast decay process ($\tau \leq 30$ ps) takes place, which corresponds to the stimulated emission transition depleting the excited-state population instantly.[14] We measured the emission spectra of the perovskite microtube laser as a function of the detection polarization angle (with respect to the tube axis). As shown in Figure 3d; Figure S12, Supporting Information, the perovskite microtube laser is linearly polarized predominantly amplifying the transverse magnetic resonant modes.
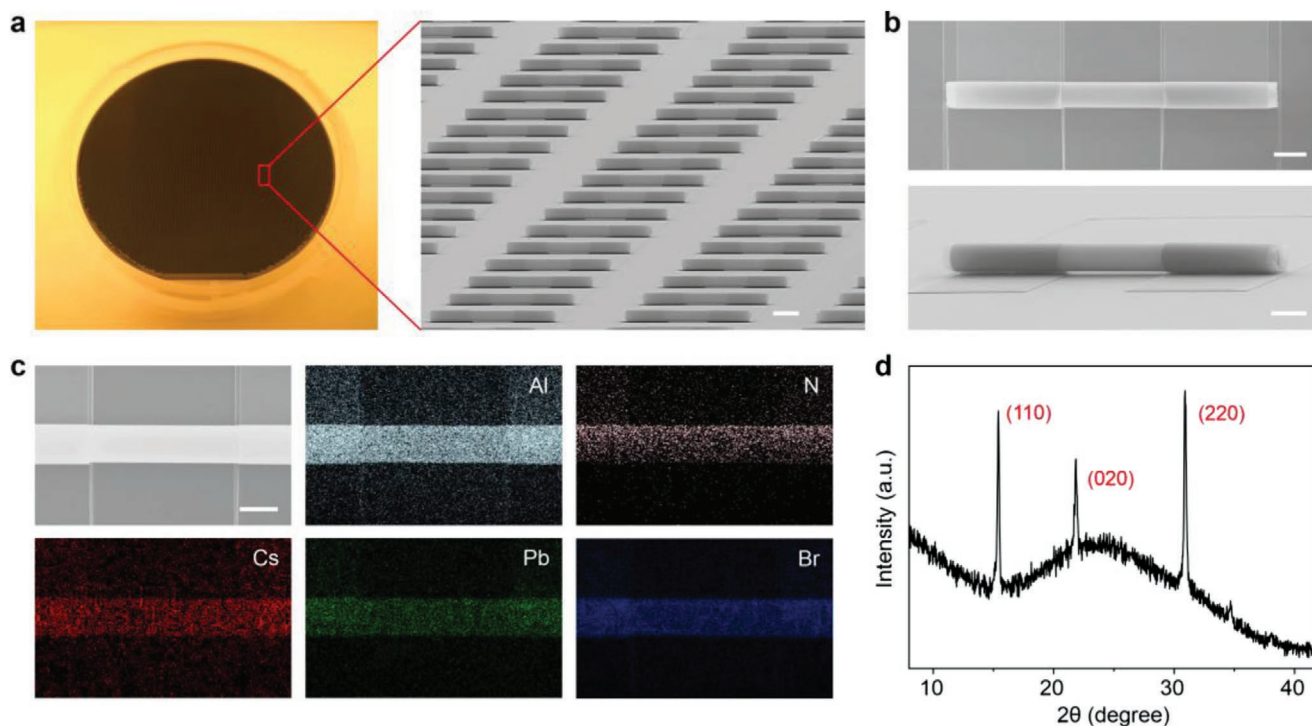
**ADVANCED
SCIENCE NEWS**
www.advancedsciencenews.com

**ADVANCED
FUNCTIONAL
MATERIALS**
www.afm-journal.de

Figure 2. Origami perovskite microtube array. a) Photograph of a 2-inch silicon wafer containing ≈2 × 10^4 CsPbBr$_3$ perovskite microtubes. Inset: SEM image of a large-area perovskite microtube array. Scale bar is 50 μm. b) SEM images of an individual perovskite microtube in top and side view. Scale bars are 25 μm. c) Magnified SEM image of a perovskite microtube and corresponding EDS mapping revealing the uniform elemental distribution of Al, N Cs, Pb, and Br. The molar ratio of Cs, Pb, and Br is 1:1:3.2. Scale bar is 20 μm. d) XRD pattern of rolled-up CsPbBr$_3$ perovskite microtubes.

Because the perovskite layer is well protected by aluminum oxide and silicon nitride films, the microtube laser exhibits excellent operation stability under ambient conditions maintaining 92.5% of its initial output intensity after a continuous excitation of 5 hours (Figure 3e). Such high operation stability is much better than that of bare perovskite lasers.[13a,b,15] Moreover, with an intrinsic spiral structure breaking the cavity rotational symmetry,[16] the perovskite microtube laser experiences directional emission behavior (Figure 3f,g). The clockwise (CW) and counterclockwise (CCW) components of the laser modes couple out of the cavity at the internal and external rolling edges, respectively. The directional laser emission facilitates efficient power output coupling, which is compulsory for almost all practical laser applications.[17] Even more interesting, each individual perovskite microtube constitutes a laser array by itself because each point at different axial positions of the microtube supports a set of optical ring resonances. We recorded the lasing spectra by scanning along the perovskite microtube (Figure 3h), which shows that the laser output wavelength is constant within an error of less than 0.1 nm. A large number of perovskite microtubes form a 2D array exhibiting almost the same laser output characteristics, for example, wavelength and polarization (Figure 3i; Figure S12, Supporting Information). Such a laser "array-in-array" is reported for the first time, which would facilitate the construction of high-density on-chip photonic integrated systems and circuits.

The origami method offers high design flexibility in both device geometry and materials composition toward programmed laser emission properties. For instance, perovskite microtubes with different diameters and therefore tunable laser modes can be fabricated in a controllable fashion. As shown in **Figure 4**a,b, with the diameter (*D*) of the perovskite microtube increasing from 15.7 to 25.5 μm, the laser mode spacing decreases from 1.78 to 1.13 nm. The laser mode spacing depends linearly on the inverse of the microtube diameter (Figure 4c) which agrees well with the WGM resonance condition.[18] Overall, the origami microtube lasers demonstrate high controllability in structure and property (Figure S13, Supporting Information). The origami method is compatible to the demands set by materials processing and microtube laser design. As shown in Figure 4d; Figure S14a,b, Supporting Information, the emission color of the microtube can be tuned by changing the halide components of the perovskite film. With CsPbCl$_{1.5}$Br$_{1.5}$, CsPbBr$_3$, and CsPbBr$_{1.5}$I$_{1.5}$ as gain media, we realized red, green, and blue (three primary colors) lasing (Figure 4e; Figure S14c–f, Supporting Information).[19] In principle, the perovskite microtube lasers can cover the full visible spectral range by further tailoring the perovskite components.[3d] Such multicolor lasers may find applications in laser lighting, displays, and imaging.

Another unique feature of the microtube cavity for lasing is the realization of 3D optical confinement along both azimuthal and axial dimensions by introducing a lobe structure onto the microtube. As shown in **Figure 5**a, a parabolic lobe structure was added to the strained bilayer pattern, which was then rolled up into a microtube cavity. The lobe structure
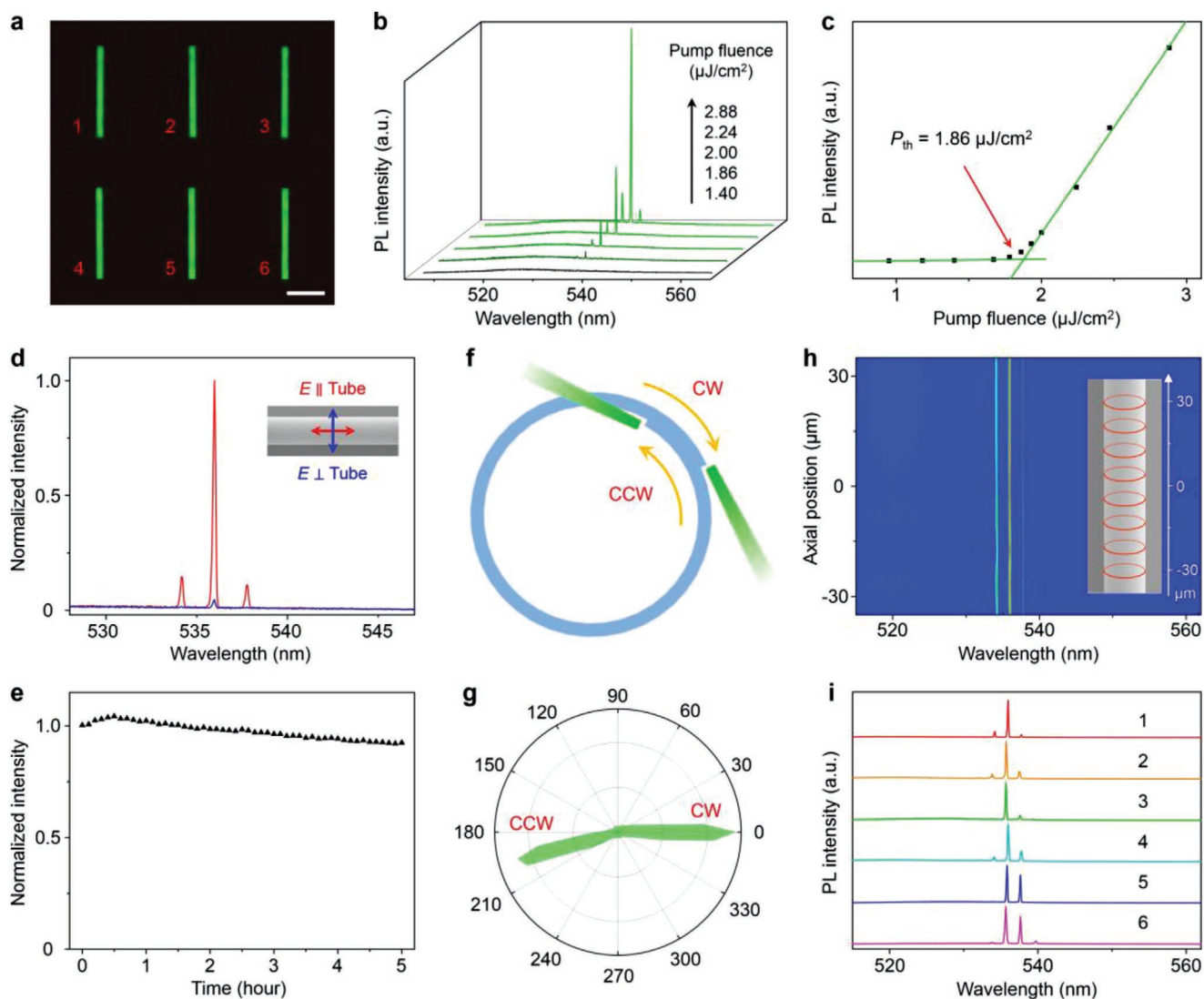
Figure 3. Laser characteristics of perovskite microtubes. a) PL image of a CsPbBr$_3$ perovskite microtube array. Scale bar is 100 µm. b) Emission spectra of an individual perovskite microtube marked as 1 in (a) under different pump fluences. c) Emission intensity as a function of pump fluence showing a clear lasing threshold of 1.86 µJ cm^{-2}. d) Polarized lasing spectra of the perovskite microtube cavity. Inset: schematic electric field direction of the emission light from microtube. e) Normalized lasing intensity of the perovskite microtube under continuous operation of 5 h at ambient conditions. f) Schematic diagram of the directional laser emission at the internal and external rolling edges. g) Far-field laser emission pattern of the perovskite microtube. h) Mapping of lasing spectra along the perovskite microtube axis. Inset: SEM image of the microtube marked with the scanning trace. i) Lasing spectra of the six perovskite microtubes in (a).

produces a parabolic refractive index gradient along the microtube axis, leading to the formation of an axial optical potential well (Figure 5b).[20] Because the axial potential well enhances the optical confinement, the 3D perovskite microtube cavity exhibits low-threshold high-Q lasing (Figure 5c). Upon introducing a lobe structure onto the perovskite microtube, the lasing threshold significantly decreases from 1.86 to 0.55 µJ cm^{-2} (Figure 5d) which is consistent with the clear increase of the cavity Q factor from 3100 to 4400 (Figure S15, Supporting Information).

Even more interesting, the axial optical potential well in the microtube cavity splits the azimuthal mode into fundamental and higher-order axial modes E_q (q is the axial mode number) (Figure 5b).[20b] As shown in Figure 5c, besides the fundamental

mode (E_0), two additional higher-order axial laser modes (E_1 and E_2) are observed. All these axial modes show low lasing thresholds (Figure 5d) and high Q factors (Figure S15, Supporting Information) compared to those in 2D confined microtube cavities. Moreover, these lasing modes show axially confined mode field distributions in the lobe region (Figure 5e), which are in good agreement with the theoretical simulations (Figure 5b). Because each axial mode interacts with the lobe edge at different positions, the CW components of the axial laser modes exhibit directional emission along different azimuths (Figure 5f). The brand-new perovskite microtube lasers with 3D directional outputs are expected to find applications in 3D photonic integration, for instance, simultaneously delivering coherent light signals for different photonic components distributed in 3D space.
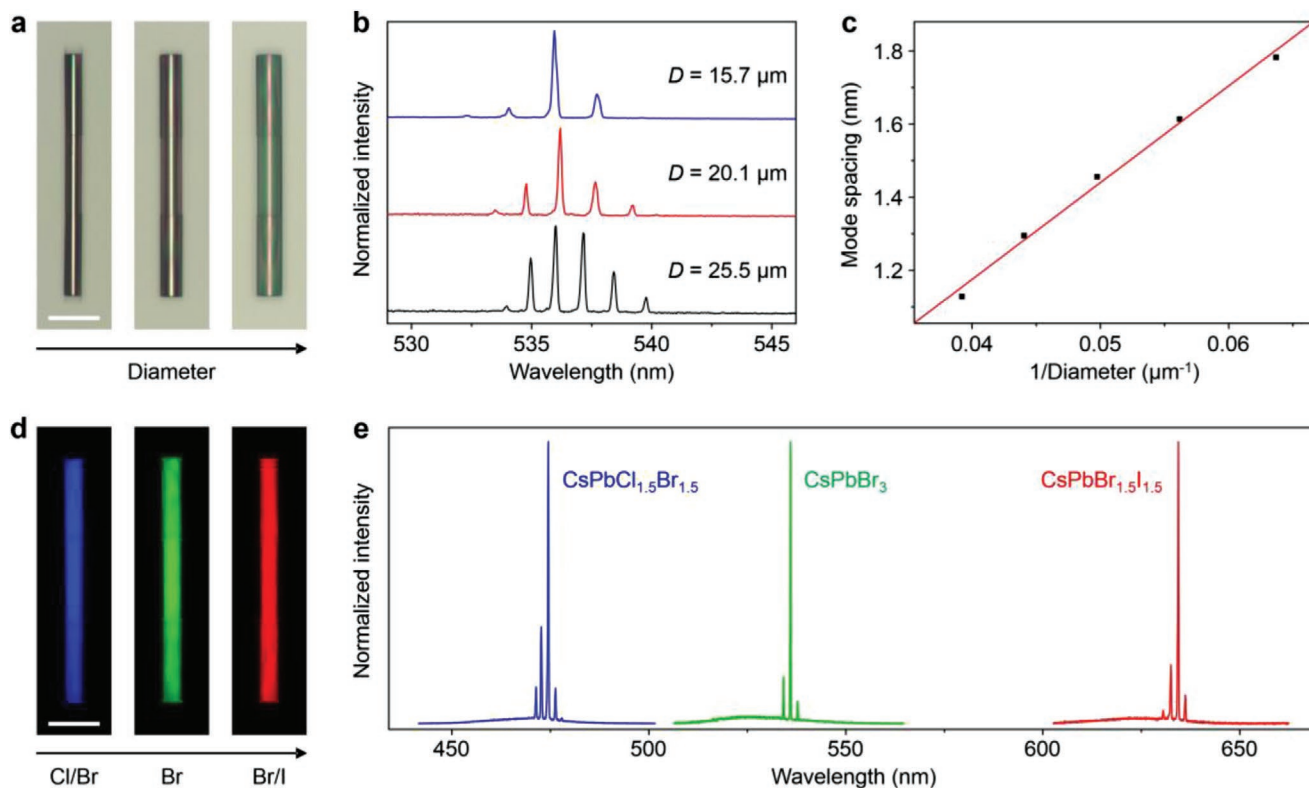
**ADVANCED
SCIENCE NEWS**
www.advancedsciencenews.com

**ADVANCED
FUNCTIONAL
MATERIALS**
www.afm-journal.de

Figure 4. Tunable laser behavior of perovskite microtubes. a) Bright-field microscopy images and b) corresponding lasing spectra of the perovskite microtubes with different diameters (D). Scale bar is 50 μm. c) Plots and linearly fitted curve of the mode spacing at ≈536.5 nm versus the inverse of microtube diameter. d) Fluorescence microscopy images and e) corresponding lasing spectra of the microtubes incorporating $CsPbCl_{1.5}Br_{1.5}$, $CsPbBr_3$, and $CsPbBr_{1.5}I_{1.5}$ perovskites. Scale bar is 50 μm.

3. Conclusion

In summary, we developed an on-chip micro-origami method for the fabrication of programmable 3D perovskite devices on wafer scale. The micro-origami method relies on standard microfabrication techniques and is thus compatible with silicon-based microelectronic and photonic system engineering. The perovskite microtubes show WGM lasing mediated by light resonating around the circular microtube cross-section. Based on the unique 3D architecture, the perovskite microtube cavities experience both superior laser performance (e.g., low threshold, directional emission, tunable output, and high stability) and new laser functionalities (e.g., laser array-in-array and 3D mode lasing). The directional laser emission facilitates efficient power output coupling for practical laser applications. The laser "array-in-array" structure allows for the construction of high-density on-chip photonic integrated systems. The 3D mode lasing with spatially dependent laser output was achieved by axial confinement. These programmable perovskite microtube lasers are expected to find use in novel 3D photonic integrated devices and systems. In principle, the micro-origami technique can also be applied to other types of devices and device geometries helping to unleash the full potential of perovskites in 3D optoelectronic and photonic applications.

4. Experimental Section

Materials: Perovskite precursors (cesium halides and lead halides) and anhydrous solvents (dimethylsulfoxide and chlorobenzene) were purchased from Sigma–Aldrich and used without any further treatment. Substrates (Prime Si + SiO$_2$ wafer, diameter = 2 inch, thickness = 280 μm, thickness of wet SiO$_2$ = 500 nm) were purchased from Microchemicals.

Preparation of Perovskite Solutions: Perovskite precursor solutions were prepared by dissolving cesium halide and lead halide with a molar ratio of 1:1 in anhydrous dimethylsulfoxide. In a typical preparation, 0.2 mм cesium halide and 0.2 mм lead halide were added in 1 mL dimethylsulfoxide, stirred at 60 °C for 2 h, and filtered with a 0.2 μm polytetrafluoroethylene filter, yielding 0.2 м perovskite precursor solutions.

Deposition of Functional Films: The silicon sacrificial layer (600 nm) and compressively strained silicon nitride layer (30, 45, 60 nm) were fabricated using chemical vapor deposition (CVD, SI 500 D, Sentech Instruments); the aluminum oxide protection layer (5 nm) and passivation layer (2 nm) were fabricated via atomic layer deposition (ALD, FlexAL, Oxford Instruments); the perovskite films (30, 45, 60 nm) were obtained through spin-coating, during which ≈1 mL anhydrous chlorobenzene was dropped onto the perovskite precursor layer, followed by annealing at 100 °C for 10 min.

Patterning of Functional Films: The spin-coated AZ 5214 E photoresist (Microchemicals) was exposed by a Maskless Aligner exposure system (MLA100, Heidelberg Instruments) and developed in AZ 726 MIF developer (Microchemicals). The obtained photoresist patterns were transferred to different functional films through reactive ion etching (RIE, Plasma Lab 100, Oxford Instruments). The aluminum oxide and perovskite films were etched by boron chloride; and the silicon and silicon nitride films, by sulfur hexafluoride.
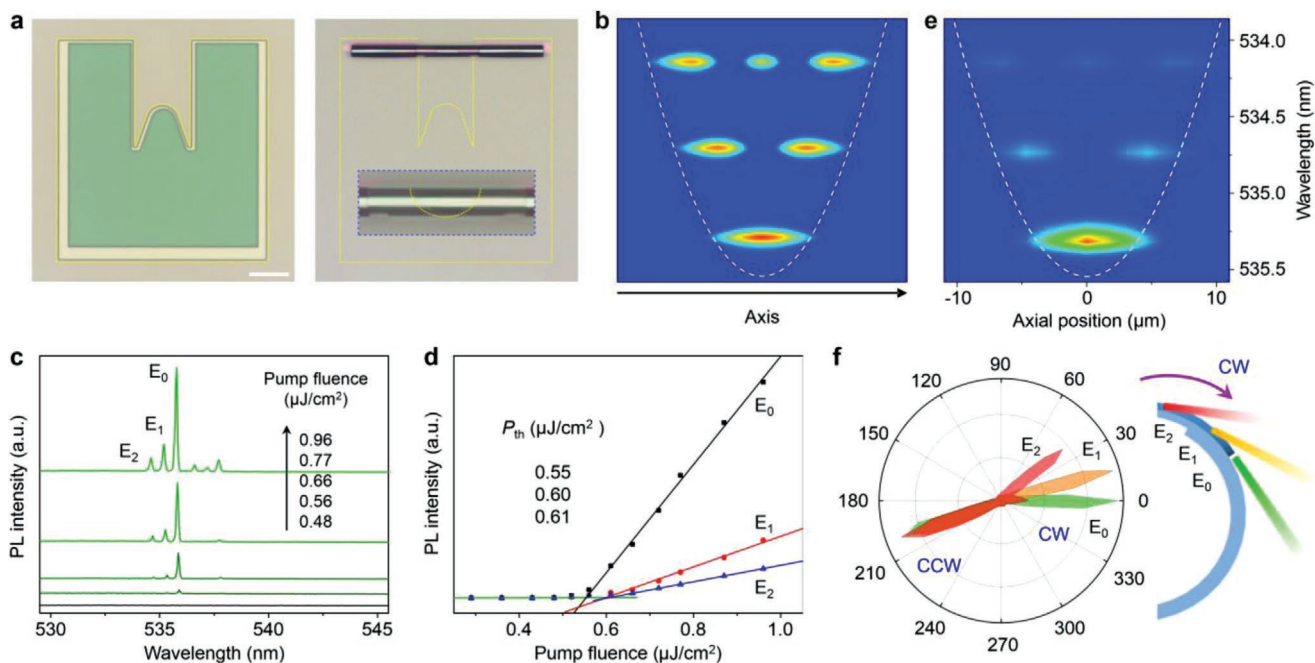
Figure 5. 3D mode lasing from a lobe-modified perovskite microtube. a) Bright-field microscopy images of a typical strained bilayer pattern with a lobe structure and the self-assembled perovskite microtube. Inset: magnified image of the middle segment of the microtube. Scale bar is 50 μm. b) Calculated field distributions of axial modes in a parabolic potential well. c) Emission spectra of a lobe-modified perovskite microtube under different pump fluences. d) Emission intensities of three axial modes as a function of pump fluence. e) Measured spatial distributions of the axial laser modes in the lobe region. f) Normalized far-field emission intensities of the axial laser modes in the lobe-modified perovskite microtube. Inset: Schematic diagram showing the directional emission of axial modes along different azimuths.

Assembling of Functional Films into Microtubes: The assembly of the strained bilayer was performed inside a xenon difluoride etching system (Xactix e2; Orbotech) and monitored in real-time with an optical microscope.

Structure Characterizations: The morphology of as-prepared perovskite microtubes was characterized by an optical microscope (Axioscope, Zeiss) and a scanning electron microscope (SEM, Hitachi SU8010). The microtube components were measured through energy-dispersive X-ray spectroscopy on the SEM. The perovskite crystal structures were examined by X-ray diffraction (XRD, PANalytical Empyrean).

Optical Measurements: The fluorescence microscopy images were taken with a microscope (FluoView-500, Olympus). The optically pumped lasing measurements were carried out using a far-field micro-photoluminescence system equipped with a mode-locked Ti:sapphire laser (Spectra Physics), a microscope, a charge-coupled device camera, and a spectrophotometer (Princeton Instruments). The time-resolved photoluminescence of the perovskite microtube laser was measured by a streak camera (C10910, Hamamatsu photonics).

Numerical Simulation: The electric field distribution of a whispering-gallery mode in a spiral microcavity was calculated with the finite element method by using COMSOL Multiphysics.

Supporting Information

Supporting Information is available from the Wiley Online Library or from the author.

Acknowledgements

Conflict of Interest

The authors declare no conflict of interest.

Data Availability Statement

The data that support the findings of this study are available from the corresponding author upon reasonable request.

Keywords

[1] a) W. Zhang, G. E. Eperon, H. J. Snaith, *Nat. Energy* **2016**, *1*, 16048; b) F. P. García de Arquer, A. Armin, P. Meredith, E. H. Sargent, *Nat.*

Rev. Mater. **2017**, *2*, 16100; c) X. K. Liu, W. Xu, S. Bai, Y. Jin, J. Wang, R. H. Friend, F. Gao, *Nat. Mater.* **2021**, *20*, 10; d) H. Dong, C. Zhang, X. Liu, J. Yao, Y. S. Zhao, *Chem. Soc. Rev.* **2020**, *49*, 951.

[2] a) D. Luo, R. Su, W. Zhang, Q. Gong, R. Zhu, *Nat. Rev. Mater.* **2019**, *5*, 44; b) Y. H. Kim, J. S. Kim, T. W. Lee, *Adv. Mater.* **2019**, *31*, 1804595; c) X. Zhang, L. Li, Z. Sun, J. Luo, *Chem. Soc. Rev.* **2019**, *48*, 517; d) K. Leng, W. Fu, Y. Liu, M. Chhowalla, K. P. Loh, *Nat. Rev. Mater.* **2020**, *5*, 482.

[3] a) B. R. Sutherland, E. H. Sargent, *Nat. Photonics* **2016**, *10*, 295; b) J. Huang, M. Lai, J. Lin, P. Yang, *Adv. Mater.* **2018**, *30*, 1802856; c) Y. Wang, H. Sun, *Small Methods* **2018**, *2*, 1700252; d) Y. Fu, H. Zhu, J. Chen, M. P. Hautzinger, X. Y. Zhu, S. Jin, *Nat. Rev. Mater.* **2019**, *4*, 169; e) Y. Jiang, X. Wang, A. Pan, *Adv. Mater.* **2019**, *31*, 1806671; f) A. P. Schlaus, M. S. Spencer, X. Y. Zhu, *Acc. Chem. Res.* **2019**, *52*, 2950; g) J. Xu, X. Li, J. Xiong, C. Yuan, S. Semin, T. Rasing, X. H. Bu, *Adv. Mater.* **2020**, *32*, 1806736.

[4] a) Q. A. Akkerman, G. Raino, M. V. Kovalenko, L. Manna, *Nat. Mater.* **2018**, *17*, 394; b) K. Wang, G. Xing, Q. Song, S. Xiao, *Adv. Mater.* **2021**, *33*, 2000306; c) Q. Zhang, Q. Shang, R. Su, T. T. H. Do, Q. Xiong, *Nano Lett.* **2021**, *21*, 3120.

[5] a) X. Qin, X. Liu, W. Huang, M. Bettinelli, X. Liu, *Chem. Rev.* **2017**, *117*, 4488; b) D. Karnaushenko, T. Kang, V. K. Bandari, F. Zhu, O. G. Schmidt, *Adv. Mater.* **2020**, *32*, 1902994; c) Y. Zhang, F. Zhang, Z. Yan, Q. Ma, X. Li, Y. Huang, J. A. Rogers, *Nat. Rev. Mater.* **2017**, *2*, 17019.

[6] a) H. Wang, H. Zhen, S. Li, Y. Jing, G. Huang, Y. Mei, W. Lu, *Sci. Adv.* **2016**, *2*, e1600027; b) Y. Yin, S. Li, S. Böttner, F. Yuan, S. Giudicatti, E. Saei Ghareh Naz, L. Ma, O. G. Schmidt, *Phys. Rev. Lett.* **2016**, *116*, 253904; c) L. B. Ma, S. L. Li, V. M. Fomin, M. Hentschel, J. B. Götte, Y. Yin, M. R. Jorgensen, O. G. Schmidt, *Nat. Commun.* **2016**, *7*, 10983; d) W. Huang, J. Zhou, P. J. Froeter, K. Walsh, S. Liu, M. D. Kraman, M. Li, J. A. Michaels, D. J. Sievers, S. Gong, X. Li, *Nat. Electron.* **2018**, *1*, 305; e) C. Becker, D. Karnaushenko, T. Kang, D. D. Karnaushenko, M. Faghih, A. Mirhajivarzaneh, O. G. Schmidt, *Sci. Adv.* **2019**, *5*, eaay7459; f) V. K. Bandari, Y. Nan, D. Karnaushenko, Y. Hong, B. Sun, F. Striggow, D. D. Karnaushenko, C. Becker, M. Faghih, M. Medina-Sánchez, F. Zhu, O. G. Schmidt, *Nat. Electron.* **2020**, *3*, 172.

[7] a) Y. Jia, R. A. Kerner, A. J. Grede, B. P. Rand, N. C. Giebink, *Nat. Photonics* **2017**, *11*, 784; b) Z. Duan, Y. Wang, G. Li, S. Wang, N. Yi, S. Liu, S. Xiao, Q. Song, *Laser Photonics Rev.* **2018**, *12*, 1700234; c) C. Qin, A. S. D. Sandanayaka, C. Zhao, T. Matsushima, D. Zhang, T. Fujihara, C. Adachi, *Nature* **2020**, *585*, 53.

[8] J. Zhao, Y. Deng, H. Wei, X. Zheng, Z. Yu, Y. Shao, J. E. Shield, J. Huang, *Sci. Adv.* **2017**, *3*, eaao5616.

[9] O. G. Schmidt, K. Eberl, *Nature* **2001**, *410*, 168.

[10] a) J. Wang, T. Zhan, G. Huang, P. K. Chu, Y. Mei, *Laser Photonics Rev.* **2014**, *8*, 521; b) C. Strelow, M. Sauer, S. Fehringer, T. Korn, C. Schüller, A. Stemmann, C. Heyn, D. Heitmann, T. Kipp, *Appl. Phys. Lett.* **2009**, *95*, 221115; c) M. H. T. Dastjerdi, M. Djavid, Z. Mi, *Appl. Phys. Lett.* **2015**, *106*, 021114; d) Y. Li, L. Feng, X. Su, Q. Li, F. Yun, G. Yuan, J. Han, *Opt. Express* **2017**, *25*, 18072.

[11] a) J. Feng, X. Yan, Y. Zhang, X. Wang, Y. Wu, B. Su, H. Fu, L. Jiang, *Adv. Mater.* **2016**, *28*, 3732; b) N. Zhang, W. Sun, S. P. Rodrigues, K. Wang, Z. Gu, S. Wang, W. Cai, S. Xiao, Q. Song, *Adv. Mater.* **2017**, *29*, 1606205; c) J.-J. Wu, H. Gao, R. Lai, M.-P. Zhuo, J. Feng, X.-D. Wang, Y. Wu, L.-S. Liao, L. Jiang, *Matter* **2020**, *2*, 1233.

[12] a) H. Dong, C. Zhang, Y. Liu, Y. Yan, F. Hu, Y. S. Zhao, *Angew. Chem., Int. Ed.* **2018**, *57*, 3108; b) C. Qiao, C. Zhang, Z. Zhou, H. Dong, Y. Du, J. Yao, Y. S. Zhao, *Angew. Chem., Int. Ed.* **2020**, *59*, 15992.

[13] a) S. W. Eaton, M. Lai, N. A. Gibson, A. B. Wong, L. Dou, J. Ma, L.-W. Wang, S. R. Leone, P. Yang, *Proc. Natl. Acad. Sci U.S.A.* **2016**, *113*, 1993; b) Y. Fu, H. Zhu, C. C. Stoumpos, Q. Ding, J. Wang, M. G. Kanatzidis, X. Zhu, S. Jin, *ACS Nano* **2016**, *10*, 7963; c) Q. Zhang, R. Su, X. Liu, J. Xing, T. C. Sum, Q. Xiong, *Adv. Funct. Mater.* **2016**, *26*, 6238; d) X. He, P. Liu, H. Zhang, Q. Liao, J. Yao, H. Fu, *Adv. Mater.* **2017**, *29*, 1604510; e) H. Zhou, S. Yuan, X. Wang, T. Xu, X. Wang, H. Li, W. Zheng, P. Fan, Y. Li, L. Sun, A. Pan, *ACS Nano* **2017**, *11*, 1189; f) C.-Y. Huang, C. Zou, C. Mao, K. L. Corp, Y.-C. Yao, Y.-J. Lee, C. W. Schlenker, A. K. Y. Jen, L. Y. Lin, *ACS Photonics* **2017**, *4*, 2281.

[14] a) S. Kéna-Cohen, S. R. Forrest, *Nat. Photonics* **2010**, *4*, 371; b) H. Dong, C. Zhang, F. J. Shu, C. L. Zou, Y. Yan, J. Yao, Y. S. Zhao, *Adv. Mater.* **2021**, *33*, 2100484.

[15] Z. Yang, J. Lu, M. ZhuGe, Y. Cheng, J. Hu, F. Li, S. Qiao, Y. Zhang, G. Hu, Q. Yang, D. Peng, K. Liu, C. Pan, *Adv. Mater.* **2019**, *31*, 1900647.

[16] a) X.-F. Jiang, C.-L. Zou, L. Wang, Q. Gong, Y.-F. Xiao, *Laser Photonics Rev.* **2016**, *10*, 40; b) J. W. Wang, Y. Yin, Y. D. Yang, Q. Hao, M. Tang, X. X. Wang, C. N. Saggau, D. Karnaushenko, X. H. Yan, Y. Z. Huang, L. B. Ma, O. G. Schmidt, *ACS Photonics* **2019**, *6*, 2537.

[17] H. Cao, J. Wiersig, *Rev. Mod. Phys.* **2015**, *87*, 61.

[18] a) S. Yang, Y. Wang, H. Sun, *Adv. Opt. Mater.* **2015**, *3*, 1136; b) G. Q. Wei, X. D. Wang, L. S. Liao, *Laser Photonics Rev.* **2020**, *14*, 2000257.

[19] Y. Fan, C. Zhang, Y. Du, C. Qiao, K. Wang, Y. Hou, Y. S. Zhao, *Adv. Funct. Mater.* **2021**, *31*, 2103031.

[20] a) P. Bianucci, S. Mukherjee, M. H. T. Dastjerdi, P. J. Poole, Z. Mi, *Appl. Phys. Lett.* **2012**, *101*, 031104; b) C. Strelow, H. Rehberg, C. M. Schultz, H. Welsch, C. Heyn, D. Heitmann, T. Kipp, *Phys. Rev. Lett.* **2008**, *101*, 127403; c) C. N. Saggau, F. Gabler, D. D. Karnaushenko, D. Karnaushenko, L. Ma, O. G. Schmidt, *Adv. Mater.* **2020**, *32*, 2003252.

2109080 (8 of 8)